ATMOSPHERIC CORRECTION OF CHRIS/PROBA DATA ACQUIRED IN THE SPARC CAMPAIGN

Luis Guanter, L. Alonso, and J. Moreno

University of Valencia - Faculty of Physics, Dr. Moliner 50, 46100, Burjassot (Valencia), Spain.
EMAIL: luis.guanter@uv.es

ABSTRACT

An atmospheric correction algorithm for satellite/airborne data taken over land has been implemented. The algorithm is designed to obtain the main atmospheric parameters needed in the correction from the image itself, so an optimal characterization of the atmospheric state, in temporal and spatial resolution terms, is achieved. The results of the application to CHRIS/PROBA data from the ESA SPARC campaign is presented in this work, focusing on the validation of both the final surface reflectance and the intermediate atmospheric water vapor and aerosol products. A final step devoted to the recalibration of the obtained reflectances is needed, due to calibration problems in the near-infrared CHRIS bands. The comparison with coincident MERIS data provides a final validation of the surface reflectance image.

Key words: Atmospheric correction, Surface reflectance, CHRIS/PROBA, Radiative transfer, SPARC campaign.

1. INTRODUCTION

In Earth Observation, the atmospheric influence on the visible and infrared radiation is strong enough to modify the reflected electromagnetic signal, causing the loss or the corruption of part of the carried information about the observed target. Thus, any set of remote sensing data needs a previous removal of the atmospheric effects in the initial processing steps, to assert a maximal accuracy and reliability in the results inferred by the latter exploitation of the data. This is the fundamental basis of the atmospheric correction in optical remote sensing: the elimination of the atmospheric effects from the useful signal reflected by the observation target in the observer's line of sight. A traditional statement of the problem can be found, for instance, in [1, 2]

Generally speaking, the atmospheric correction procedure can be divided into two separated phases. The first one is devoted to the retrieval of the atmospheric parameters needed to quantify the atmospheric influence on the measured radiation. Once the atmospheric optical functions are known, the second phase deals with the decoupling of the surface and atmosphere radiative transfer effects, which leads to the evaluation of equations formulating the Top-of-Atmosphere (TOA) radiances as a combination of surface and atmosphere contributions. Depending on the degree of accuracy of the physical assumptions underneath these formulations, there is a wide range of equations to be solved, ranging from simple analytical equations to complex integro-differential ones that have to be solved using numerical techniques.

Concerning the first phase, the loadings and types of the atmospheric components, gases and aerosols, must be known in order to calculate their optical properties. For an accurate atmospheric correction, the ideal situation would be the availability of an atmospheric product containing the main atmospheric information simultaneous to the image acquisition and with the same spatial resolution. This can be accomplished if atmospheric retrievals are done from the data itself, by means of the inversion of the measured radiances in some selected wavelengths. Thanks to the hyperspectral and multiangular capabilities of the last generation of satellite sensors, the extraction of atmospheric information from the data themselves is becoming a real possibility.

In this framework, we have developed an atmospheric correction algorithm for high spectral resolution data over land surfaces. It is designed to obtain the main atmospheric parameters needed in the correction from the image itself, so an optimal characterization of the atmospheric state, in temporal and spatial resolution terms, is achieved. The use of the limiting concept of dark targets is avoided in the aerosol retrievals. Instead, the atmospheric parameters are estimated from every type of land surfaces, with the only restriction that the surface reflectance can be represented by a linear combination of two pure vegetation and bare soil endmembers.

The algorithm has already been applied to the recently launched ESA sensors CHRIS/PROBA [3] and ENVISAT/MERIS [4] with a high consistency in the results. In this paper we describe the particular implementation of the algorithm for CHRIS/PROBA data, as well as the results obtained in the estimation of atmospheric parameters and the subsequent surface reflectance retrieval. The validation of these results is achieved by means of simultaneous ground measurements made during the ESA Spectra-Barrax Campaign (SPARC), which took place in Barrax (Spain) during 12-14th July, 2003.

Proc. of the 2nd CHRIS/Proba Workshop, ESA/ESRIN, Frascati, Italy
28-30 April (ESA SP-578, July 2004)

2. CHRIS/PROBA DATA

The Project for On-Board Autonomy (PROBA) [3] small satellite mission launched on 22 October 2001 is a technology proving experiment to demonstrate the on-board autonomy of a generic platform suitable for small scientific or application missions. The instrument payload includes the Compact High Resolution Imaging Spectrometer (CHRIS).

The platform provides pointing in both across-track and along-track directions, as well as a fixed scanning speed on the ground during imaging in order to increase the CHRIS integration time. In this way, the system CHRIS/PROBA has multiangular capabilities, acquiring five consecutive images at time when the zenith angle of the platform with respect to the "fly-by position" (position where the satellite projection in the surface is closest to the observation target), corresponding to a minimum observation zenith angle (MZA), is equal to a set of Fly-by Zenith Angle (FZA): 0°, ±36°, ±55°. Negative values correspond to target locations East of the ground track. CHRIS datasets from the SPARC campaign present an $MZA = +20°$ on 12th July, and a $MZA = -27°$ on 14 July. This means that the image closest to nadir, $FZA = 0°$, is acquired with a view zenith angle equals to 20°.

CHRIS operates over the visible/NIR bands from 400 nm to 1050 nm and can operate in 62 spectral bands at a spatial resolution of 34 m, or with 18 bands at 17 m, with a minimum spectral sampling interval ranging between 1.25 (@400 nm) and 11 nm (@1000 nm). There are several operation modes, with different combinations of band configuration (number, center location and width) and spatial resolution. The data we have worked with correspond to mode 1, consisting of 34 m pixel and 62 bands between 400 and 1000 nm.

3. ALGORITHM DESCRIPTION

3.1. Estimation of Atmospheric Parameters

In the spectral range covered by the algorithm, 0.4-1.0 μm, we consider three atmospheric contributors to be treated specifically: ozone, water vapor and aerosols. The resultant content values are used to calculate the corresponding spectral atmospheric reflectance and transmittance functions with the 6S radiative transfer code [5]. These functions are an input in the second algorithm step to finally obtain the surface reflectance.

The stratospheric ozone absorbs principally in the shorter wavelengths. Due to its low spatial and temporal variation, we do not make a particular treatment of this gas, as the total ozone column content can be provided with enough accuracy by any public database. For instance, the values provided by the ECMWF (European Center for Medium-Range Weather Forecasting) are attached to ENVISAT/MERIS images.

For water vapor and aerosols the situation is different, as they vary strongly in small spatial and temporal scales. So, the temporal and spatial coincidence of this atmospheric information and the image to be processed is needed. The most efficient way to achieve this is the retrieval of the atmospheric parameters from the image itself.

There are several methods to retrieve aerosols and water vapor from high spectral resolution data, but the general approach is to calculate them separately (see, e.g., [6–9] for aerosol retrieval and [10–13] for water vapor). However, due to the coexistence of aerosols and water vapor in the same low atmosphere layers ($\sim$ 2-3 km), the coupling can be important: aerosols radiative effects are noticeable in the near-infrared (NIR) bands if middle-big size aerosols are present, coupling to absorption in those wavelengths close to the water vapor absorption band centered around 0.94 μm.

So, we have implemented a procedure which retrieves aerosols and water vapor contents simultaneously. The retrieval is based on the assumption that the atmospheric state is invariant inside a 30×30 km window (or the whole image for sensors with swath less than 30 km, as CHRIS), while the surface reflectance varies from pixel to pixel. This one is given by a linear combination of two vegetation and soil spectra, which act as endmembers. Then, aerosol and water vapor contents are retrieved simultaneously from 5 pixels inside this window, by means of a multiparameter inversion of the TOA spectral radiances from a selected combination of bands, chosen depending on the particular band configuration of each sensor.

This inversion is performed by means of the minimization of a Merit Function δ^2 specifically designed for this problem,

$$\delta^2 = \sum_{pix=1}^{5} \sum_{\lambda_i} \frac{1}{\lambda_i^2} \left[\rho_{TOA}|_{pix,\lambda_i} - \rho_{SIM}|_{pix,\lambda_i} \right]^2 \quad (1)$$

where ρ_{SIM} is the TOA reflectance simulated with the 6S code, λ_i corresponds to the center of the i band in the particular band configuration of the sensor, and ρ_{TOA} stands for the TOA apparent reflectance measured by the sensor, given in terms of the TOA radiance L_{TOA}, the solar constant E_{sc} and the cosine of the solar zenith μ_s angle by

$$\rho_{TOA} = \frac{\pi L_{TOA}}{\mu_s E_{sc}}. \quad (2)$$

The free parameters in the optimization are the water vapor column content, the aerosol loading and the percentage of basic types, and the proportions of vegetation and soil endmembers for each of the 5 reference pixels.

The particular selection of 5 as the number of pixels to serve as a reference for the atmospheric retrievals is a balance between the computation burden and the representative sampling in the 30×30 km window: a higher number would increase the number of free parameters in the inversion, without adding too much information to the sampling. The 5 reference pixels must have a spectral contrast as strong as possible (ranging from pixels with high vegetation content to high soil content) in order to improve the numerical stability in the inversion process. A perfect choice for the set of reference pixels would be a pure vegetation pixel, a pure bare soil pixel, and three intermediate ones, mixture of vegetation and soil.

The Merit Function in Eq. 1 is weighted by λ_i^{-2} to drive the inversion towards the smaller wavelengths, where the effect of the aerosols is bigger, while the reflectance of most of the natural surfaces is lower. The set of wavelengths used for the inversion is selected depending on the sensor. For CHRIS, calibration problems have been found in the NIR channels, so the last 10 bands (for the 62 bands mode 1) are not used. The noisy first band in the extreme of the focal plane array is also discarded.

For the construction of the simulated TOA apparent reflectance ρ_{SIM}, CHRIS bands are reproduced using rectangular filter functions, and the surface is assumed to be Lambertian, what leads to the expression:

$$\rho_{TOA}(\mu_s, \mu_v, \phi) = t_g \left[\rho_0 + \frac{T\uparrow T\downarrow \rho_s}{1 - S\rho_s} \right], \quad (3)$$

where t_g is the transmittance due to gases; ρ_0 is the intrinsic atmospheric reflectance, also called atmospheric path reflectance; ρ_s is the surface reflectance; S is the spherical albedo, reflectance of the atmosphere for isotropic light entering it from the surface; μ_v is the cosine of the view zenith angle; ϕ is the relative azimuth between the Sun and viewing directions; $T\uparrow$, $T\downarrow$ are, respectively, the upward and downward total atmospheric transmittances (for diffuse + direct radiation), in the illumination and observation directions. The angular dependencies of t_g, ρ_0, $T\uparrow$ and $T\downarrow$ have been omitted for the sake of simplicity.

Neglecting the directional effects in the target reflectance provides a simple formulation of the radiative transfer, what leads to an important decrease in the computation time and modelling effort. It has been demonstrated that the Lambertian approach can work well in the general case where the acquisition geometry is not in the retro-dispersion hot spot direction [14], and so if the observation is close to nadir. Thome *et al.* [15] states that the percentage difference between the Lambertian case and typical non-Lambertian cases is less than 1% in the near nadir viewing range. So, in order to reduce the errors associated to this approach, the atmospheric retrievals are performed from the image acquired with the view zenith angle closer to nadir (in PROBA nomenclature, Fly-by Zenith Angle (FZA) equals to 0°), and the corresponding atmospheric transmittance and reflectance functions in Eq. 3 needed to derive the surface reflectance are calculated then for each one of the acquisition angles.

For aerosol characterization, the SRA types defined by the Radiation Commission of IAMAP [16] (dust-like, water soluble, oceanic and soot) are implemented in the 6S database. So, aerosols are specified by means of the visibility and the percentages of those basic types, resulting in 4 free parameters.

Regarding water vapor, the total column content is another free parameter to be inverted. The vertical profile is given by the U.S. Standard Atmosphere [17], also implemented in the 6S database. The ozone profile is set by this default atmosphere as well.

The surface spectral reflectance is given by the linear combination of two endmembers of typical vegetation (alfalfa) and soil spectra,

$$\rho_s = C_v \rho_{veg} + C_s \rho_{soil} \qquad C_v, C_s \in [0, 1.5] \quad (4)$$

The proportions of vegetation and soil are allowed to be bigger than 1.0 in case spectra brighter than the endmembers are present. The ten coefficients $C_{v,s}$, 2 for each of the 5 pixels, are also free parameters in the TOA reflectance simulation.

The minimization of the Merit Function in Eq. 1 is performed by the Powell's Minimization Method [18], based on a 1–D minimization separately in each direction of the parameters space, without the need of the analytical expression of the function derivatives. An appropriate initialization of the Powell's algorithm is needed in order to reduce the convergence time and to reach the best minimum. For the atmospheric parameters, common values are selected: visibility 23 km, a mixture of continental and maritime model for aerosol type and a water vapor column content of 2.0 g·cm^{-2}. Concerning the vegetation and soil proportions, a strong correlation between the *Normalized Difference Vegetation Index* (NDVI) [19] and the coefficients $C_{v,s}$ was found from several simulations.

3.2. Surface reflectance retrieval

General Procedure: Lambertian assumption

Once the atmospheric functions are calculated, they are used to retrieve the surface reflectance image from the TOA radiance image provided by the sensor. As starting point, a Lambertian reflectance for the surface is assumed, what leads to the analytical inversion of Eq. 3 to retrieve ρ_s. So, an initial surface reflectance image is obtained with a little algebra.

This is an important justification for the Lambertian assumption. However, some authors have pointed out that this assumption may lead to noticeable errors in some particular combinations of geometry,

target reflectance and atmospheric state conditions [20, 21]. The problem is that multiangular information is needed in order to characterize properly the BRDF effects in the target. In the case of platforms with multiangular viewing capabilities, such as PROBA, accounting for the directional effects in the target reflectance is feasible. Then, although the general procedure is based on the Lambertian assumption also for CHRIS/PROBA, a further step involving directional effects has been done for some pixels in the image.

BRDF/Atmosphere Coupling Correction

In order to consider directional effects in the target, instead of Lambertian behavior, Eq. 3 can be extended to account for the BRDF coupling between atmosphere and surface reflectance [22]. However, the resultant formulation is not analytically invertible to retrieve ρ_s, because this is embedded in integrals accounting for the atmosphere/surface coupling terms (surface hemispherical-directional, directional-hemispherical and hemispherical-hemispherical reflectances, angular integrals of the downward radiance field and the surface BRDF). Then, for the evaluation of the coupling terms ρ_s is, in turn, needed. We have then an integral equation, which may be solved by an iterative process.

Thus, there is a need for techniques that can provide some surface information, to be used in the calculations of the coupling terms. In practical considerations, there are several ways to get these initial estimates of the surface reflectance. Most of them depend on the availability of other surface products, but some authors [20, 23] have suggested surface BRDF information can be retrieved from an initial correction assuming a Lambertian surface, where coupling terms are not needed. The angular pattern retrieved by means of the Lambertian assumption is fitted to a BRDF model, which is used to perform the integrals in the coupling terms. Once the coupling terms are known, a newer set of ρ_s angular values is obtained. This is again used to update the coupling terms and the subsequent ρ_s values. The procedure continues in this fashion until convergence in two consecutive iterations is found.

The BRDF model we use to fit the angular pattern ρ_s in each iteration is the RPV model [24], which offers a good balance between number of free parameters, three, and flexibility in the representation of distinct BRDF shapes. The retrieved angular pattern is fitted to RPV model by means of the Powell's Minimization Method, and the angular integrals for the coupling terms are numerically calculated with the Gaussian quadratures method. The final output of this BRDF coupling correction is a second order correction of the surface reflectance obtained from the Lambertian assumption, more substantial in the larger observation angles. A detailed description of the procedure is given in [25].

From an operational point of view, the application of this procedure to a set of images, as it should be in the case of the CHRIS/PROBA 5 angles, is quite complex:

- The fit to the RPV model is computationally very expensive on a pixel by pixel basis (even if a linear kernel model was chosen instead). So, the time needed in each iteration would be prohibitive for practical applications.
- The geometric correction of the images has an associated error of around three pixels, what corresponds to around 100 m in the surface. As a result, it is not very rigorous to assume 5 viewing directions for every single point, because the value corresponding to one angle might be referred to a point in the neighborhood of the observation point for another angle. Particularly, this leads to important problems in the evaluation of the borders of different surfaces in the images, as different angles might be viewing different surfaces, in both sides of the boundaries.
- There is only a partial overlapping in the observed region for the 5 images, so an initial test of the number of angles needed to perform an adequate BRDF correction should be done for those areas not viewed from all of the angles.

For these reason, the BRDF correction has only been made for some pixels in the CHRIS/PROBA images, taken visually from the center of uniform surfaces in the overlapped region, to avoid the problems with the geometric correction. Anyway, directional effects do not cause important modifications of the results obtained with the Lambertian assumption, as expected for a geometric configuration out of the principal plane, what reinforces the use of the Lambertian approach.

Adjacency Correction

The final step in our atmospheric correction algorithm is the removal of the image blurring caused by those photons reflected by the target environment and scattered by the atmosphere particles into the sensor's line-of-sight. This effect is called *adjacency effect* because the apparent signal at the TOA of a pixel comes also from adjacent pixels.

The adjacency correction involves inverting the linear combination of reflectances to isolate the reflectance of the target pixel. The simple formulation proposed by Vermote *et al.* [20, 26], weighting the strength of the adjacency effect by the ratio of diffuse to direct ground-to-sensor transmittance, is used:

$$\rho_s = \rho_s^u + \frac{t_d(\mu_v)}{e^{-\tau/\mu_v}}[\rho_s^u - \bar{\rho}], \tag{5}$$

where ρ_s^u is the surface reflectance before the adjacency treatment, ρ_s the final surface reflectance,

output of the complete atmospheric correction algorithm, and $\bar{\rho}$ is the average of the environment reflectance. This average is calculated for a 1×1 km^2, which is in the same order of the aerosol coupling scale.

4. RESULTS

4.1. Atmospheric Retrievals

Once the algorithm has been properly implemented and tested with simulated data, it has been applied to real CHRIS/PROBA data. The ESA SPARC campaign (*SPectra bARrax Campaign*) [27, 28] has been very important in the validation of the algorithm, as it offered a unique situation in which CHRIS/PROBA images were acquired simultaneously to atmospheric and ground in-situ measurements. The SPARC campaign took place in Barrax, La Mancha, Spain, from 12 to 14 of July 2003, under the umbrella of a formal ESA campaign as part of Phase-A Preparations for the SPECTRA mission. We have two sets of CHRIS/PROBA images from that date (12th and 14th July 2003, acquired in mode 1, 62 bands and 34 m). The results obtained from the application of the algorithm to those images and the validation with in-situ measurements will be discussed next.

Starting with the atmospheric retrievals, 5 reference pixels have been selected according to the criterium of having a maximum spectral contrast: one pixel from a potato field, two from corn, one from alfalfa and the last one from bare soil. Concerning the inversion of the TOA radiances for the 5 reference pixels in order to estimate the atmospheric information, from a quick look to Fig. 1 it may be noted that some discrepancies happen between the TOA radiance spectra and the fitted ones. Dashed circles show the wavelengths where the fits are worst. The bands in the extremes of the spectral range are among them. This was a priori expected due to the detectors in the borders of focal plane arrays usually present problems, because the maximum performance for array detectors is chosen to be in the center of the array. Other wavelengths with possible calibration problems are around 0.5 and 0.85 μm: in the first case, either a *binning* problem, shifts in the spectral positions of the narrow bins which compose a band, or a bad implementation of the filter functions may explain the apparition of two peaks between 0.48 and 0.52 μm.

Despite these problems, the information in the rest of bands is enough to lead to reliable results. The water vapor column contents for 12 and 14 July are compared with the values provided by radiosoundings launched simultaneously to PROBA overpasses in Table 1. The errors are around 13% taking radiosoundings as a reference, what is a good result if the high spatial variability of water vapor and the CHRIS calibration problems mentioned are considered.

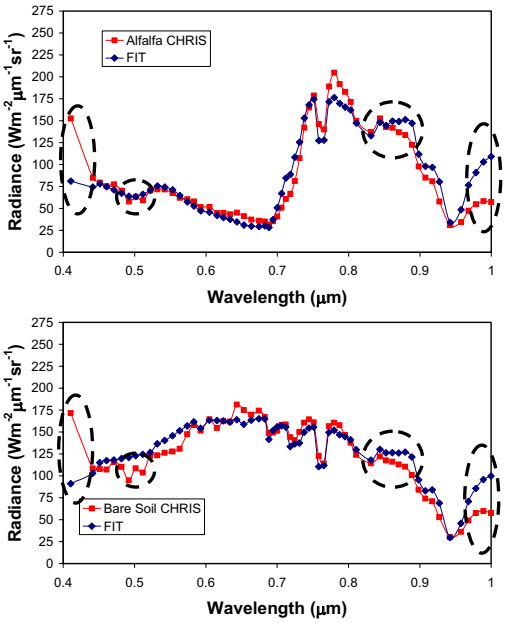

Figure 1. Fits of 2 of the 5 reference pixels for the aerosols and water vapor retrieval corresponding to the FZA= 0° image of 12 July 2003. Dashed circles point the wavelengths with major deviations.

Table 1. Comparison between the water vapor column contents retrieved from CHRIS data and the integration of simultaneous radiosoundings.

	Retrieved values	**Radiosounding**
12/7	1.62 g·cm^{-2}	1.46 g·cm^{-2}
14/7	1.82 g·cm^{-2}	1.61 g·cm^{-2}

Concerning aerosols retrieval, the calculated parameters are displayed in Table 2. The visibility values are around those found in normal atmospheric conditions. However, we can state that the algorithm seems to not be very sensible to aerosol types, because the retrieved values are very close to the initialization values. Anyway, these values are not very different from those expected in Barrax (rural and possible Mediterranean maritime aerosols).

Table 2. Aerosol parameters retrieved from CHRIS/PROBA data. VIS stands for visibility, DL for dust-like type, WS for water soluble, OC for oceanic and SO for soot.

	VIS	**%DL**	**%WS**	**%OC**	**%SO**
12/7	26.9 km	14.4	39.4	40.0	6.2
14/7	17.8 km	16.2	39.8	40.0	4.0

Ground solar irradiance spectra, global and direct radiation, have been used to validate the retrieved aerosol parameters. In Fig. 2 the ground measurements, taken simultaneously to the image acquisition by a LICOR detector[1], are compared with runs of the 6S code under the same conditions, setting aerosol specification to the values in Table 2.

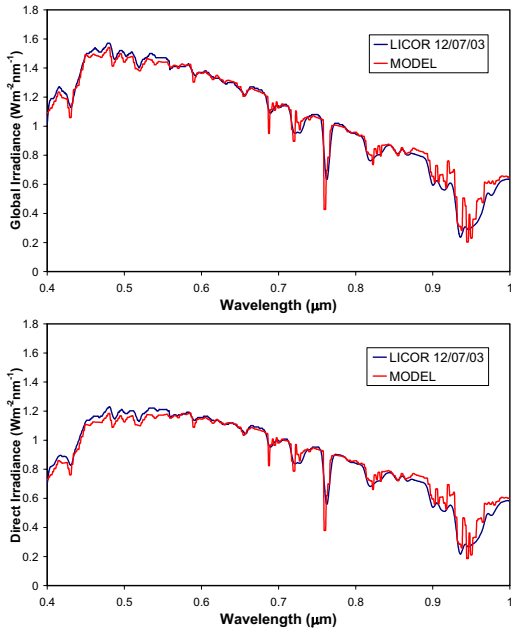

Figure 2. Comparison of 6S code simulated total and direct irradiances using the retrieved atmospheric parameters as input with ground measurements (12/07/03).

4.2. Surface Reflectance Retrieval

Surface reflectance spectra for 2 of the 5 reference pixels obtained from the retrieved atmospheric parameters and Eq. 3 are plotted in Fig. 3, as well as the TOA apparent reflectance.

It can be stated that not only several systematic small artifacts are present in the corrected spectra, but also the typical plateau shape for vegetation spectra is lost. From a close look at these artifacts in the 5 spectra, one can note that, despite looking like some random noise, they have a systematic fluctuation, with a similar spectral variation. Thus, a procedure eliminating these oscillations should provide a set of spectral multiplicative coefficients to be applied to every spectrum after the atmospheric correction. We have called this procedure *recalibration*, as it has similitude with in-flight calibration procedures to convert digital numbers to radiances [29,30].

4.3. Surface Reflectance Recalibration

To find a spectral recalibration curve, there is a need for reference patterns to be used in the calculation of

[1]Data from the Solar Radiation Unit of the University of Valencia

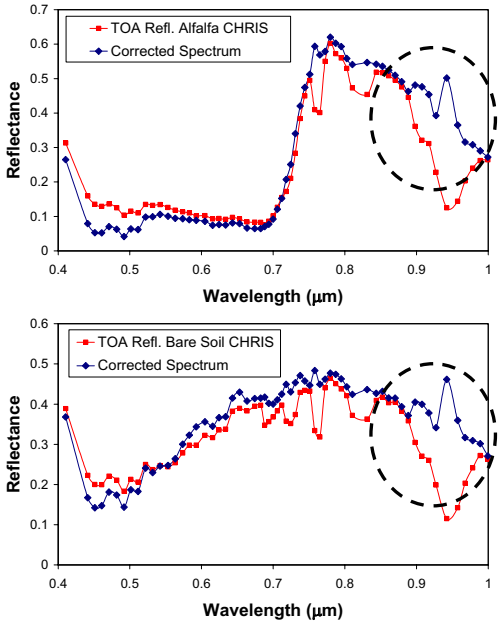

Figure 3. Surface and TOA apparent reflectances for 2 of the 5 reference pixels obtained from Eq. 3 and the atmospheric information in Tables 1 and 2. Dashed circles shows a systematic loss of the expected shape in the NIR wavelengths.

the multiplicative coefficients. This is usually done by means of ground measured spectra, taken with a relative temporal coincidence with the image acquisition. However, these spectra are seldom available, except for data from ground campaigns.

As the requirement is to have some reference surface spectra free from artifacts and with the same reflectance levels, we can use the surface reflectance spectra constructed by the atmospheric retrieval module, avoiding the limiting use of ground measurements: the $C_{v,s}$ coefficients calculated as a by-product in the atmospheric retrievals can be used with Eq. 4 to calculate a surface reflectance spectrum free from the spikes for each one of the 5 reference pixels. Then, thanks to the systematism in the oscillations, a correlation can be derived between spiky and smooth spectra, given the recalibration coefficients as a result. For each band, the recalibration coefficients are the slope of the linear fit of the 5 points (one for each reference pixel) corresponding to the comparison between the smooth and the spiky reflectances.

The resultant recalibration curves for the 5 angles are shown in Fig. 4. The curve obtained from the MODTRAN4 simulations is also plotted. Several conclusions can be extracted from Fig. 4:

- The recalibration not only removes little artifacts, but it also reconstructs the expected shape in the NIR wavelengths, with a recalibration reaching a factor 2. The correction in the first band is important as well. This confirms the

a priori expectations, because the focal plane array is designed to have the best radiometric quality in the central wavelengths, getting worse as the wavelength approaches the extremes.

- The spikes in the corrected spectra are not due to intrinsic inaccuracies in the correction algorithm, because the spectral position and signs of the peaks in the recalibration curves are different in those from MODTRAN4 and CHRIS data. If there were a systematic miscalculation of the atmospheric functions, it would have been detected in both simulations and real data.

- The recalibration curve is nearly angle independent, as the different curves are almost overlapped. This reinforces the validity of the coefficients as universal coefficients to be applied in a vicarious calibration of the raw TOA data.

- Both the general shape and the levels of the recalibration curve are in very good agreement with the one provided by Sira Technology Ltd, the designers of the instrument (M. Cutter, personal communication), calculated from an engineering perspective.

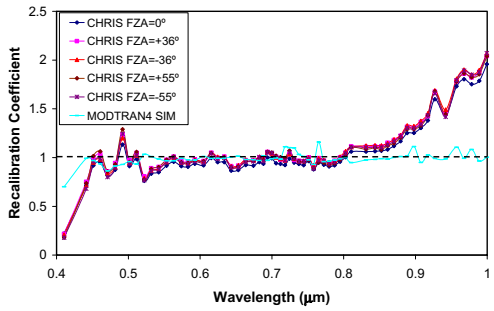

Figure 4. Recalibration curve for the 5 CHRIS/PROBA angles (12th July) and the MODTRAN4 simulations.

The surface reflectance after the recalibration for the 5 reference pixels is shown in Fig. 5. The results are highly satisfactory, as the spikes have been completely removed, and the vegetation plateau in the NIR is also recovered. Only in the bands between 0.95 and 1 μm some artifacts are still visible, due to the perturbation caused by the influence of plants water content, as well as the mentioned high degradation of the detectors response. This results in an overestimation of the reflectance in these bands in the case of soil surfaces, what would be difficult to improve.

Each recalibration curve is applied to the corresponding image after the atmospheric correction. Fig. 6 displays a true color composition of the TOA and corrected images for FZA= 0° from 12 July. Both are plotted using the same color scale. From a quick look at them, an important decrease of the blue level is found in the corrected image, due to the removal of molecular and particle scattering in the shorter

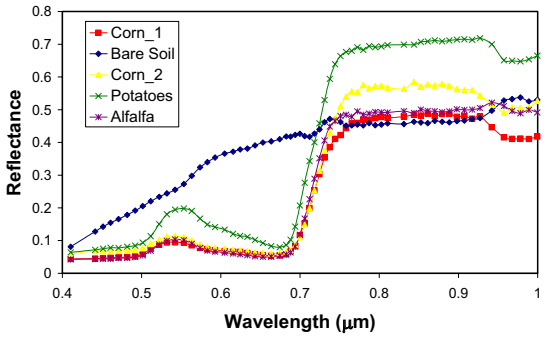

Figure 5. Surface reflectances for the 5 reference pixels after the application of the corresponding recalibration curve.

wavelengths. An increase in the contrast is also appreciable thanks to the treatment of the adjacency effects.

Figure 6. TOA and corrected images (FZA= 0°) from 12 July. The red frame points outs the Barrax study site.

The algorithm basis is general enough to be applied to different sensors with little modifications in the implementation. Thanks to this, it is being used to correct small windows from MERIS images. Even though the spatial resolution is completely different, some corrected spectra from CHRIS and MERIS have been compared in Fig. 7. To avoid problems with sub-pixel mixing, the spectra have been extracted from uniform zones in the image. The agreement in the results is high, even with the differences in calibration and technical capabilities of both sen-

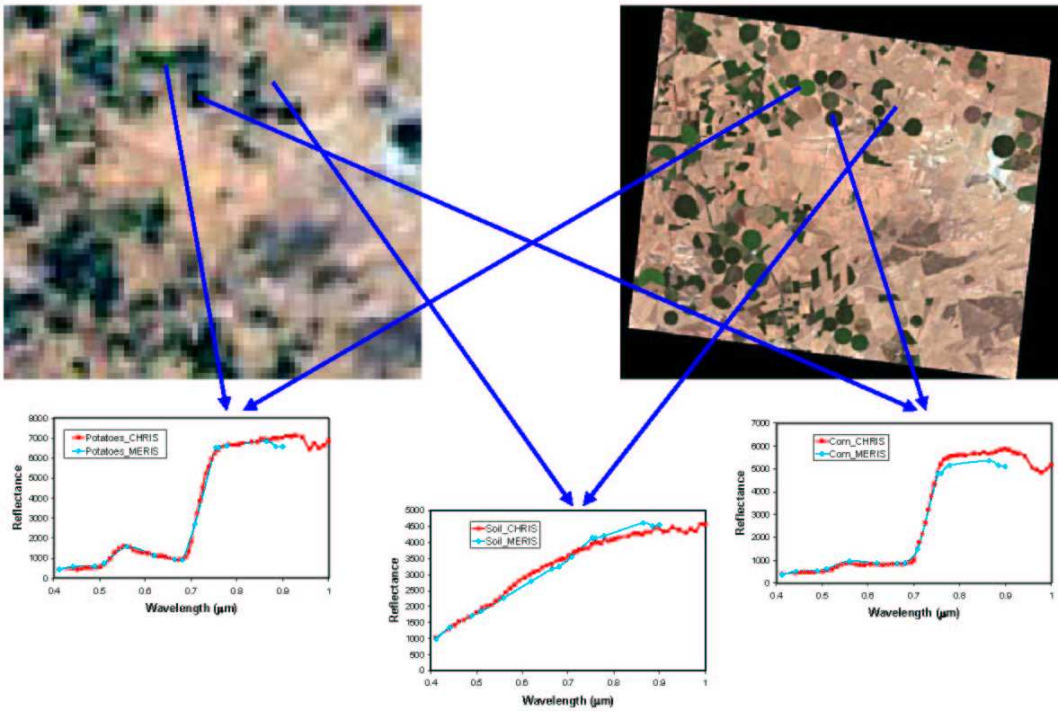

Figure 7. Comparison between CHRIS and MERIS corrected spectra from Barrax, 14 July. Reflectance in Y-axis are multiplied by 10^4.

sors, which demonstrates the algorithm's reliability and consistency.

5. CONCLUSIONS

A new atmospheric correction algorithm for satellite data taken over land has been presented in this work. The fundamental basis lies on the estimation of the main atmospheric parameters from the data to be corrected, what provides an accurate characterization of the atmospheric state simultaneous to the image acquisition.

The strategy followed for the retrieval of the atmospheric information avoids the limiting use of dark targets, so the algorithm can be applied to a wide range of land surfaces, from dense forests to arid areas.

A polishing/recalibration curve for the smoothing of the retrieved surface reflectance is automatically calculated by the algorithm, without needing external ground measurements as a reference. This curve accounts for both small inaccuracies in radiative transfer calculations and calibration problems of the sensor.

Real CHRIS/PROBA data present important calibration problems, specially in NIR wavelengths. Radiances are underestimated in such spectral range. Anyway, the information for atmospheric characterization seems to be enough, as stated by means of the comparison of the retrieved atmospheric products with ground measurements taken during the ESA SPARC campaign. The recalibration procedure fixes calibration problems, leading to smooth surface reflectance spectra with the typical flat plateau shape in NIR for pure vegetation pixels. A comparison with surface reflectance spectra derived from MERIS data provides a validation of the recalibration procedure and of the complete algorithm, as the surface reflectances retrieved from each sensor are quite similar and no recalibration is applied to MERIS data.

REFERENCES

[1] R. S. Fraser, "Computed atmospheric corrections for satellite data," in *Conf. Scanners and Imagery Systems for Earth Resources Observations*, Proc. SPIE **51**, pp. 64, 1974.

[2] Y. J. Kaufman, "The atmospheric effect on remote sensing and its correction," in *Theory and Applications of optical Remote Sensing*, Wiley, 1989.

[3] CHRIS/PROBA Web Page: www.CHRIS–PROBA.org.uk

[4] ESA, *ENVISAT MERIS Product Handbook*, Issue 1.1, December 2002.

[5] E. F. Vermote, D. Tanré, J. L. Deuzé, M. Herman, and J. J. Morcrette, "Second Simulation of the Satellite Signal in the Solar Spectrum, 6S: An overview," *IEEE. Trans. Geosci. Remote Sensing.* **GE-35**, pp. 675–686, May 1997.

[6] B. Holben, E. Vermote, Y. J. Kaufman, D. Tanré, and V. Kalb, "Aerosol retrieval over land from

AVHRR data - Application dor atmospheric correction," *IEEE. Trans. Geosci. Remote Sensing.* **GE-30**, pp. 212–222, March 1992.

[7] Y. J. Kaufman, D. Tanré, L. A. Remer, E. F. Vermote, A. Chu, and B. N. Holben, "Operational remote sensing of tropospheric aerosol over land from EOS moderate resolution imaging spectroradiometer," *J. Geophys. Res.* **102**, pp. 17051–17067, 1997.

[8] W. von Hoyningen-Huene, M. Freitag and J. P. Burrows, "Retrieval of aerosol optical thickness over land surfaces from top-of-atmosphere radiance," *J. Geophys. Res.* **108**, pp. 4260–4279, 2002.

[9] J. V. Martonchik, D. J. Diner, R. A. Kahn, T. P. Ackerman, M. M. Verstraete, B. Pinty, and H. R. Gordon, "Techniques for the retrieval of aerosol properties over land and ocean using multiangle imaging," *IEEE. Trans. Geosci. Remote Sensing.* **GE-36**, pp. 1212–1227, July 1998.

[10] D. Schlapfer, C. C. Borel, J. Keller, and K. I. Itten, "Atmospheric pre-corrected differential absorption technique to retrieve columnar water vapor," *Remote Sens. Environ.* **65**, pp. 353–366, 1998.

[11] P. Chylek, C. C. Borel, W. Clodius, P. A. Pope and A. P. Rodger, "Satellite-based columnar water vapor retrieval with the multi-spectral thermal imager (MTI)," *IEEE. Trans. Geosci. Remote Sensing.* **GE-41**, pp. 2767–2770, 2003.

[12] M. Vesperini F. M. Breon, and D. Tanre, "Atmospheric Water Vapor Content from Spaceborne POLDER Measurements," *IEEE Trans. Geosci. Remote Sens.* **37**, pp. 1613–1619, 1999.

[13] J. Fischer and R. Bennartz, *Retrieval of total water vapour content from MERIS measurements.* ESA reference number PO-TNMEL- GS-005, ESA-ESTEC, Noordwijk, Netherlands, Algorithm Theoretical Basis Document (ATBD), 1997.

[14] J. Settle, "On the dimensionality of multi-view hyperspectral measurements of vegetation," *Rem. Sens. Environ.* **90**, pp. 235–242, 2004.

[15] K. Thome, F. Palluconi, T. Takashima, and K. Masuda, "Atmospheric correction of ASTER," *IEEE Trans. Geosci. Remote Sens.* **36**, pp. 1199–1211, 1998.

[16] World Meteorological Organization, *A preliminary cloudless standard atmosphere for radiation computation*, WCP-112, World Climate Research Program, CAS, Radiation Commission of IAMAP, Boulder, Colorado, 1986.

[17] R. A. Mc Clatchey, R. W. Fenn, J. E. A. Selby, F. E. Volz and J. S. Garing, "Optical properties of the Atmosphere," AFCRL-TR- 71-0279, *Enviro. Research papers* **354**, L.G. HANCOM FIEL Bedford, Mass. U.S.A., 1971.

[18] W. H. Press, B. P. Flannery, S. A. Teukolosky, and W. T. Vetterling, *Numerical Recipes*, Cambridge University Press, 1986.

[19] C. O. Justice, J. G. R. Townshend, B. N. Holben and C. J. Tucker, "Analysis of the phenology of global vegetation using meteorological satellite data," *Int. J. Remote Sensing* **6**, pp. 1271–1318, 1985.

[20] E. F. Vermote, N. El Saleous, C. O. Justice, Y. J. Kaufman, J. L. Privette, L. Remer, J. C. Roger, and D. Tanré, "Atmospheric correction of visible to middle infrared EOS-MODIS data over land surface: Background, operational algorithm and validation," *J. Geophys. Res.* **102**, pp. 17131–17141, 1997.

[21] T. Y. Lee, and Y. J. Kaufman, "Non-lambertian effects in remote sensing of surface reflectance and vegetation index," *IEEE. Trans. Geosci. Remote Sensing.* **GE-24**, pp. 699–708, May 1986.

[22] D. Tanré, M. Herman, and P. Y.Deschamps, "Influence of the atmosphere on space measurements of directional properties," *App. Opt.* **21**, pp. 733–741, May 1983.

[23] B. Hu, W. Lucht and, A. H. Strahler, "The interrrelationship of atmospheric correction of reflectances and surface BRDF retrieval: a sensitivity study," *IEEE. Trans. Geosci. Remote Sensing.* **GE-37**, pp. 724–738, March 1999.

[24] H. Rahman, B. Pinty, and M. M.Verstraete, "Coupled surface-atmosphere reflectance (CSAR) model, 2. Semiempirical surface model usable with NOAA advanced very high resolution radiometer data," *J. Geophys. Res.* **98**, pp. 20791–20801, 1993.

[25] L. Guanter, J. M. Martí, and J. F. Moreno, "Atmospheric correction algorithm for multiangular satellite measurements in the solar spectrum", in *Conf. Remote Sensing*, Proc. SPIE, Barcelona (Spain), 2003.

[26] R. Richter, "A spatially adaptative fast atmospheric correction algorithm," *Int. J. Remote Sensing* **17**, pp. 1201–1214, 1996.

[27] J. Moreno, "The SPECTRA Barrax Campaign (SPARC): Overview and first results from CHRIS data," *This issue.*

[28] SPARC Web Page: http://io.uv.es/projects/sparc/

[29] R. Richter, "On the in-flight absolute calibration of high spatial resolution spaceborne sensors using small ground targets," *Int. J. Remote Sensing* **18**, pp. 2827–2833, 1997.

[30] R. Santer, X. F. Gu, G. Guyot, J. L. Deuze, C. Devaux, E. Vermote, and M. Verbrugghe, "SPOT calibration at the La Crau Test Site (France)," *Remote Sens. Environ.* **41**, pp. 227–237, 1992.